J. Fluid Mech. (2006), *vol.* 562, *pp.* 405–414.
doi:10.1017/S0022112006001406 Printed in the United Kingdom

Statistics of subgrid-scale stress states in homogeneous isotropic turbulence

By SERGEI G. CHUMAKOV

Center for Nonlinear Studies, Los Alamos National Laboratory, Los Alamos, NM 87544, USA
chumakov@lanl.gov

(Received 20 January 2006 and in revised form 15 June 2006)

Two parameters are introduced that uniquely characterize the state of a third-order symmetric tensor. We show that the proposed parameters arise from the uniform metric in the matrix space; thus the joint PDF of these parameters can be used to determine the geometrical statistics of any third-order symmetric tensor. We use this joint PDF to describe the states of the subgrid-scale stress, which is of central interest in large-eddy simulation. Direct numerical simulation of forced isotropic turbulence is used in our *a priori* tests. With the proposed parameterization we can also assess the most probable flow configuration at the scales of motion just above the Kolmogorov scale. We test four different subgrid-scale models in terms of how well they predict the structure, or state, of the subgrid-scale stress. It is found that models based on truncated Taylor series do not produce an adequate distribution of states, even if augmented by a turbulent viscosity term. On the other hand, models based on the scale-similarity assumption predict a distribution of states that is close to actual.

1. Introduction

Classification of small-scale motions in turbulent flows is of central importance in large-eddy simulation (LES). Recent developments in this direction relied on analysis of the strain-rate tensor S_{ij}, its eigenvalues and the geometrical relationship between the principal strain directions and flow characteristics such as vorticity (Kerr 1985; Ashurst *et al.* 1987; Nomura & Post 1998; Nomura & Diamessis 2000) and helicity (Kerr 1987).

In incompressible flow, the state of S_{ij} can be classified with a single parameter such as the normalized intermediate eigenvalue (Kerr 1985; Ashurst *et al.* 1987) or a certain algebraic expression involving its eigenvalues α, β and γ, such as

$$s^* = \frac{-3\sqrt{6}\alpha\beta\gamma}{(\alpha^2+\beta^2+\gamma^2)^{3/2}}. \tag{1.1}$$

Equation (1.1) was mentioned by Kerr (1987) and later by Lund & Rogers (1994), who used it to estimate the most probable strain state in the isotropic turbulence, the axisymmetric expansion ($s^* = 1$). Also, s^* can describe the state of the deviatoric part of the subgrid-scale (SGS) stress in LES, $\tilde{\tau}_{ij} \equiv \tau_{ij} - \delta_{ij}\tau_{kk}/3$ (Tao, Katz & Meneveau 2002; Higgins, Parlange & Meneveau 2003; Kang & Meneveau 2005). Here $\tau_{ij} = \overline{u_i u_j} - \bar{u}_i \bar{u}_j$, and the overbar denotes spatial filtering.

The most attractive feature of s^* is that, unlike other normalizations, it is uniformly distributed in the space of traceless symmetric matrices, which will be shown below. This property implies that the lines of constant s^* (computed from the eigenvalues of S_{ij}) divide the Lumley triangle (Lumley & Newman 1977) in a uniform way, as noted by Lund & Rogers (1994).

In this paper, we formally start with the uniform metric in the space of 3×3 symmetric tensors and arrive at two parameters that characterize the state of a symmetric tensor. One of these parameters is equivalent to s^* and characterizes the deviatoric part of the tensor, while the other corresponds to the dilatational part. Using joint probability density functions (PDFs) of these parameters we can investigate the full distribution of states of the SGS stress τ_{ij}, as well as the states predicted by different classes of SGS models.

2. A uniform measure of the stress state

The state of a symmetric stress A_{ij} is characterized by a point (α, β, γ) in the space of its eigenvalues. If one is interested only in the structure of the stress with no regard of the magnitude, one need consider only the unit sphere in the eigenvalue space $A_{ii}^2 = \alpha^2 + \beta^2 + \gamma^2 = 1$, reducing the number of parameters to two. Naturally, one would like to introduce these two parameters s^* and q^* in such a way that $\mathrm{d}s^* \, \mathrm{d}q^* \propto \mathrm{d}\mu_A = \mathrm{d}A_{11} \, \mathrm{d}A_{12} \, \mathrm{d}A_{13} \, \mathrm{d}A_{22} \, \mathrm{d}A_{23} \, \mathrm{d}A_{33}$.

It can be shown that the measure $\mathrm{d}\mu_A$ in the space of A_{ij} translates into the measure $\mathrm{d}\mu = |V(\alpha, \beta, \gamma)| \, \mathrm{d}\alpha \, \mathrm{d}\beta \, \mathrm{d}\gamma$ in the eigenvalue space, where $V(\alpha, \beta, \gamma) = (\alpha - \beta)(\beta - \gamma)(\gamma - \alpha)$ is the Vandermonde determinant (Mehta 2004, Chap. 3). In order to simplify the expression, we use the linear coordinate transformation $[\alpha, \beta, \gamma]^T = \boldsymbol{Q}[x, y, z]^T$, where orthogonal matrix $\boldsymbol{Q}$ is defined as

$$\boldsymbol{Q} = \begin{bmatrix} 2/\sqrt{6} & 0 & 1/\sqrt{3} \\ -1/\sqrt{6} & 1/\sqrt{2} & 1/\sqrt{3} \\ -1/\sqrt{6} & -1/\sqrt{2} & 1/\sqrt{3} \end{bmatrix}.$$

In the (x, y, z) coordinate system, $|V(\alpha, \beta, \gamma)|$ simplifies to $|y(3x^2 - y^2)|/\sqrt{2}$. We now change to the spherical coordinates given by $x = r\cos\phi\cos\theta$, $y = r\cos\phi\sin\theta$, $z = r\sin\phi$, $0 \leqslant \theta < 2\pi$, $-\pi/2 \leqslant \phi \leqslant \pi/2$, to obtain $|V(\alpha, \beta, \gamma)| = r^3/\sqrt{2}|\sin 3\theta|\cos^3\phi$. Thus the measure $\mathrm{d}\mu_A$ in the space of A_{ij} translates into the measure $r^3|\sin 3\theta| \cos^4\phi \, \mathrm{d}r \, \mathrm{d}\theta \, \mathrm{d}\phi$ in the (r, θ, ϕ) space, which induces the measure $|\sin 3\theta| \cos^4\phi \, \mathrm{d}\theta \, \mathrm{d}\phi$ on the unit sphere $r = 1$. Furthermore, we can confine our investigations to one-sixth of the whole sphere $(0 \leqslant \theta \leqslant \pi/3)$ by reordering the eigenvalues so that $\alpha \geqslant \beta \geqslant \gamma$ without biasing the distribution of the states.

Now we define two parameters s^* and q^* as

$$s^* = -\cos 3\theta, \qquad q^* = \frac{1}{6\pi}(12\phi + 8\sin 2\phi + \sin 4\phi), \tag{2.1}$$

with the angles θ and ϕ given by

$$\cos\theta = \frac{3\tilde{\alpha}}{\sqrt{6}(\tilde{\alpha}^2 + \tilde{\beta}^2 + \tilde{\gamma}^2)^{1/2}}, \qquad \sin\phi = \frac{\alpha + \beta + \gamma}{\sqrt{3}(\alpha^2 + \beta^2 + \gamma^2)^{1/2}},$$

where $\tilde{\alpha} = \alpha - A_{ii}/3$, $\tilde{\beta} = \beta - A_{ii}/3$, $\tilde{\gamma} = \gamma - A_{ii}/3$ are the eigenvalues of $\tilde{A}_{ij}$, the deviatoic part of A_{ij}. One can also express s^* and q^* in terms of the tensor invariants:

$$s^* = \frac{-\sqrt{6}\tilde{A}_{ii}^3}{\left(\tilde{A}_{jj}^2\right)^{3/2}}, \tag{2.2}$$

$$q^* = \frac{1}{3\pi}(6\sin^{-1} W + 2W(5 - 2W^2)\sqrt{1 - W^2}), \tag{2.3}$$

where $A_{ii}^2 = A_{ij}A_{ji}$, $A_{ii}^3 = A_{ij}A_{jk}A_{ki}$ and $W = A_{ii}/\sqrt{3A_{jj}^2}$.

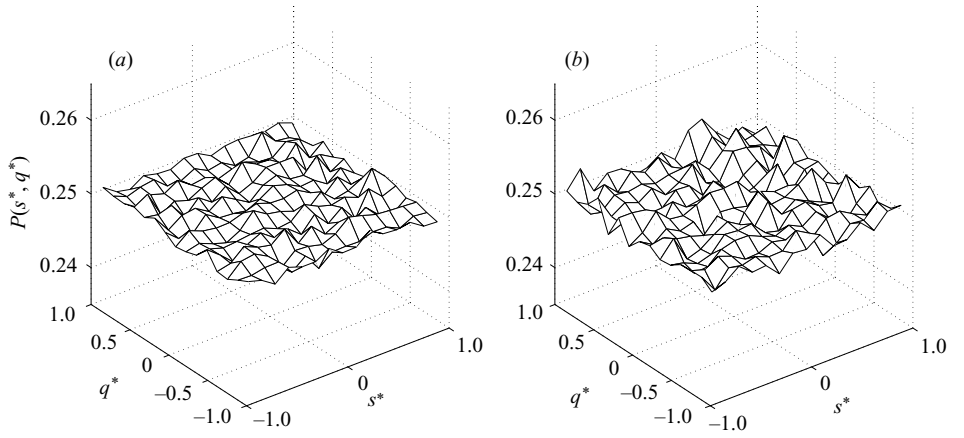

FIGURE 1. The joint PDF of (s^*, q^*) for two random matrix fields: (*a*) Gaussian and (*b*) uniform.

Parameters s^* and q^* satisfy $(s^*, q^*) \in [-1, 1]^2$, and $\mathrm{d}s^* \, \mathrm{d}q^* \propto \mathrm{d}\mu_A$. The latter enables us to use the joint PDF $P(s^*, q^*)$ to evaluate the distribution of the states of any symmetric tensor, and in particular, the SGS stress tensor τ_{ij}.

As an illustration, figure 1 shows $P(s^*, q^*)$ for two sets of randomly defined A_{ij}: (*a*) the Gaussian distribution with density $\exp(-A_{ii}^2/2)$, and (*b*) the uniform distribution in the intersection of the subspace of symmetric matrices with the unit ball in the Frobenius norm $\|A\| = (A_{ij}A_{ij})^{1/2}$. Figure 1 shows a uniform distribution of states for both cases, which illustrates that $P(s^*, q^*)$ is not biased towards any particular state.

Expression (2.2) was introduced by Kerr (1987) and later by Lund & Rogers (1994), without a formal proof of s^* being uniformly distributed in the space of symmetric traceless matrices. Subsequently s^* was used to characterize the state of $\tilde{\tau}_{ij}$ by Tao *et al.* (2002), Higgins *et al.* (2003) and Kang & Meneveau (2005). We advocate using the pair (s^*, q^*) instead of just s^* to fully characterize the state of τ_{ij}, since it is rarely traceless.

3. Statistics of SGS stress states

We are now in a position to examine the distribution of states of the SGS stress τ_{ij}. This is done using direct numerical simulation (DNS) of forced, isotropic, homogeneous turbulence in periodic box. The SGS stress is extracted from the fully resolved field using a Gaussian filter function, and the joint PDF $P_\tau(s^*, q^*)$ is constructed.

The incompressible Navier–Stokes equations were solved in a periodic box with sides of length $L = 2\pi$ and $N = 256$ grid points in each direction. A standard pseudo-spectral algorithm was used, fully de-aliased by a combination of truncation and phase shifting (Livescu, Jaberi & Madina 2000). The turbulence is sustained by a deterministic forcing term given by Machiels (1997). The condition $k_{\max}\eta \geqslant 1.8$ was satisfied for all times to ensure that all important flow scales are resolved (Pope 2000). Here $k_{\max} = N\sqrt{2}/3$ is the maximum significant wavenumber resolved by the grid, and η is the Kolmogorov length scale. The average Reynolds number based on the Taylor microscale was $R_\lambda \approx 130$.

Figure 2 shows contour plots of $P_\tau(s^*, q^*)$ for two filter sizes, $\Delta = 2\pi/64$ and $2\pi/16$. Since we used a Gaussian filter, τ_{ij} is positive semi-definite (Ghosal 1999) and thus

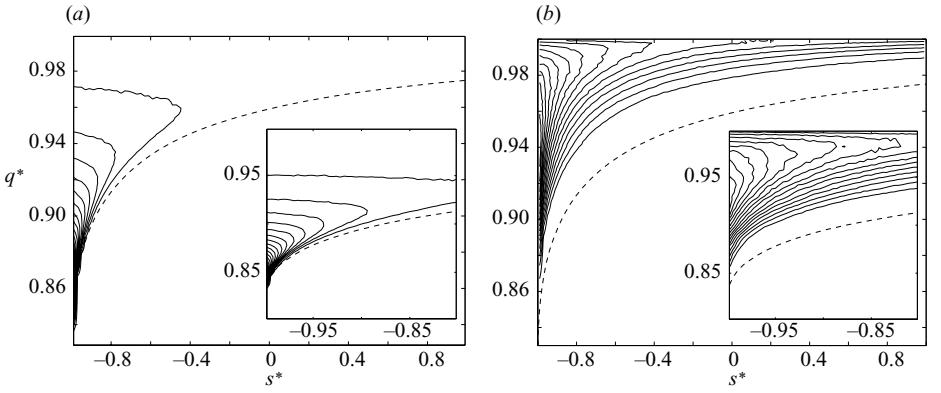

FIGURE 2. Contour plot of $P_\tau(s^*, q^*)$ for two filter sizes: (*a*) $\Delta = 2\pi/64$, (*b*) $\Delta = 2\pi/16$. The dashed line shows the boundary of the region that corresponds to positive definite matrices. Fifteen contours are shown, equally spaced from 9.3 to 139.1 in (*a*), and from 3 to 46.2 in (*b*).

points (s^*, q^*) must lie above the dashed line that shows the boundary of the region of positive definite matrices.

Using the data, we can find the most probable SGS flow configuration. The most probable value of s^* is -1 (similar to Tao *et al.* 2002), and it does not seem to depend on the filter size. The most probable value of q^* grows with Δ, indicating that for isotropic turbulence the averaged subgrid scales become more isotropic for larger Δ. On the other hand, when Δ is reduced the peak of $P_\tau(s^*, q^*)$ shifts closer to the dashed curve. With $s^* \approx -1$ this indicates that for small filter size the SGS structures are highly anisotropic, namely, two eigenvalues of τ_{ij} are much smaller than the third, which corresponds to two smooth and one strongly fluctuating velocity component.

4. *A priori* evaluation of SGS models

In this Section, we examine the distribution of states of τ_{ij} predicted by four models: the Smagorinsky model, nonlinear model, mixed model and dynamic structure model. The choice of models was motivated by the fact that they take the structure of the modelled term from different sources: the resolved strain-rate tensor, resolved deformation tensor, a combination of the two, and a Leonard tensor associated with test filtering.

The Smagorinsky model (Smagorinsky 1963) is given by

$$\tau_{ij}^s = -2(C_s\Delta)^2|\bar{\boldsymbol{S}}|\bar{S}_{ij}, \qquad |\bar{\boldsymbol{S}}| = \sqrt{2\bar{S}_{ij}\bar{S}_{ij}}, \tag{4.1}$$

where $\bar{S}_{ij} = (1/2)(\partial\bar{u}_i/\partial x_j + \partial\bar{u}_j/\partial x_i)$ is the resolved strain-rate tensor and C_s is a user-defined constant that can be assigned manually or computed via the dynamic procedure of Germano *et al.* (1991).

The nonlinear model is defined as (Leonard 1974; Bardina, Ferziger & Reynolds 1980)

$$\tau_{ij}^{nl} = C_{nl}\Delta^2 \frac{\partial\bar{u}_i}{\partial x_k}\frac{\partial\bar{u}_j}{\partial x_k}, \tag{4.2}$$

or $\boldsymbol{\tau} = \bar{\boldsymbol{D}}\cdot\bar{\boldsymbol{D}}^T$ where $\bar{\boldsymbol{D}}$ is the deformation tensor. It gives excellent results in *a priori* testing (see Liu, Meneveau & Katz 1994; Borue & Orszag 1998) but leads to an inevitable blow-up in *a posteriori* testing (Leonard 1997) due to an effective negative

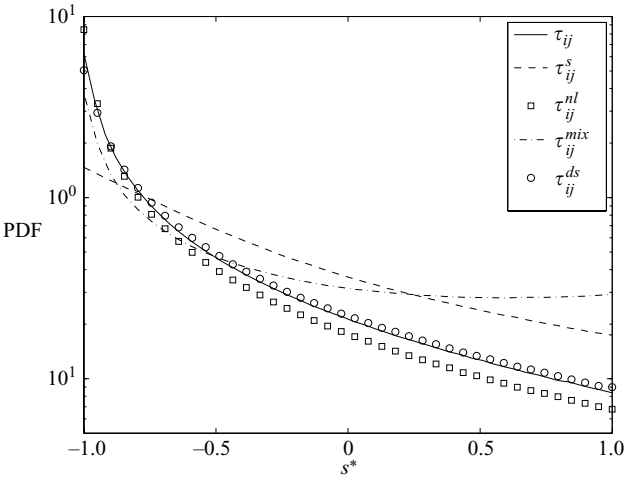

FIGURE 3. PDF of s^* for SGS stress and four models: Smagorinsky, nonlinear, mixed and dynamic structure; $\Delta = 2\pi/32$.

viscosity in at least one direction everywhere in the computational domain. To ensure stability, Bardina *et al.* (1980) proposed augmenting the nonlinear model by an eddy viscosity term. This leads to the mixed model, given by

$$\tau_{ij}^{mix} = C_{nl}\Delta^2 \frac{\partial \bar{u}_i}{\partial x_k}\frac{\partial \bar{u}_j}{\partial x_k} - 2(C_s\Delta)^2|\bar{\boldsymbol{S}}|\bar{S}_{ij}. \tag{4.3}$$

There are several ways to evaluate the scaling constants C_{nl} and C_s. We adopt the dynamic procedure described by Kang, Chester & Meneveau (2003), with the test filter size $\hat{\Delta} = 2\Delta$.

The dynamic structure (DS) model is a one-equation LES model given by (Goutorbe, Laurence & Maupu 1994; Pomraning & Rutland 2002)

$$\tau_{ij}^{ds} = \frac{2k_{sgs}}{L_{kk}}L_{ij}. \tag{4.4}$$

Here, $k_{sgs} = \tau_{ii}/2$ is the SGS kinetic energy, $L_{ij} = \widehat{\bar{u}_i\bar{u}_j} - \hat{\bar{u}}_i\hat{\bar{u}}_j$ is the Leonard tensor and the hat denotes the test filtering. Since k_{sgs} is not available from the resolved field, it has either to be modelled or obtained from a separate transport equation. This model can be regarded as a scale-similarity model with specific scaling factor. It gives encouraging *a priori* and *a posteriori* results in terms of quality of prediction and stability of calculations (Pomraning & Rutland 2002; Chumakov & Rutland 2005).

It should be noted that the first three models contain derivatives of the filtered flow field. To be consistent in our *a priori* tests we project the filtered flow field on to coarse LES grid with grid spacing equal to $\hat{\Delta}$ before evaluating the derivatives.

Since the Smagorinsky model gives $q^* \equiv 0$, we start by comparing the distributions of s^* only. This is done in figure 3 for the filter size $\Delta = 2\pi/32$. Other filter sizes produce similar plots (not shown). It is apparent from the figure that the most frequent state of $\tilde{\tau}_{ij}$ is axisymmetric contraction, in agreement with Tao *et al.* (2002). Based on the figure, Smagorinsky and mixed models tend to under-predict the peak in the distribution while having a larger tail, in contrast with the nonlinear models which over-predict the peak. The dynamic structure model seems to give the most plausible prediction.

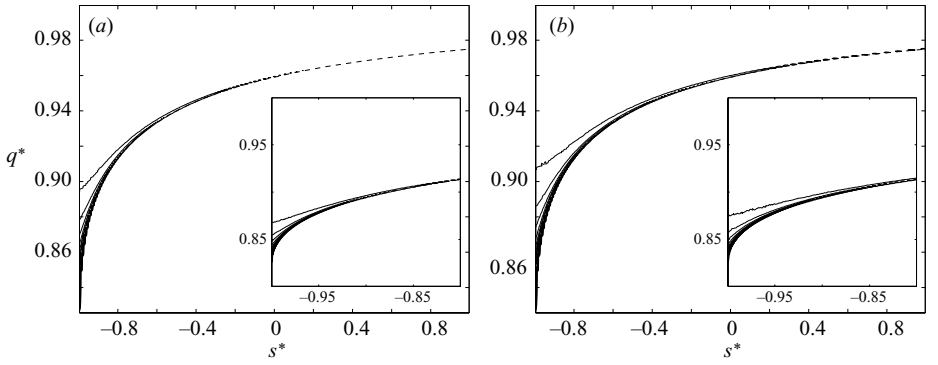

FIGURE 4. Contour plot of $P_{\tau^{nl}}(s^*, q^*)$ for two filter sizes: (*a*) $\Delta = 2\pi/64$, (*b*) $\Delta = 2\pi/16$. The dashed line shows the boundary of the region that corresponds to positive definite matrices. Fifteen contours are shown, equally spaced from 17.5 to 261.9 in (*a*), and from 13.3 to 199.5 in (*b*).

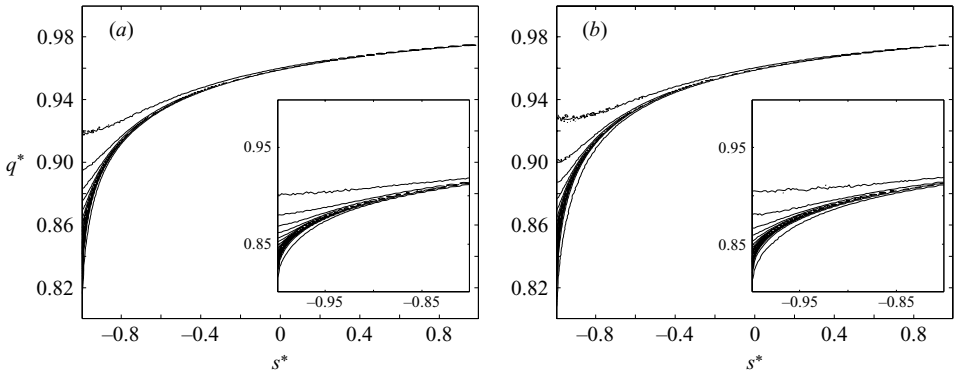

FIGURE 5. Contour plot of $P_{\tau^{mix}}(s^*, q^*)$ for two filter sizes: (*a*) $\Delta = 2\pi/64$, (*b*) $\Delta = 2\pi/16$. The ratio of test and base filter sizes is equal to 2. Fifteen contours are shown, equally spaced from 7.0 to 105.0 in (*a*), and from 4.8 to 70.4 in (*b*).

Figures 4, 5 and 6 show the contour plots of joint PDF of (s^*, q^*) predicted by the nonlinear, dynamic mixed and DS models. It can be seen from figure 4 that the nonlinear model, although it predicts the correct trend for the s^*-distribution (figure 3), fails to predict the correct dilatation. A possible explanation of this is that the eigenvalues of τ_{ij}^{nl} are squares of the singular values of the resolved deformation tensor $\bar{D}_{ij}$. Since $\bar{D}_{ij}$ is traceless, it is possible that the smallest of its singular values is much smaller than the largest. This produces the eigenvalues (α, β, γ) of τ_{ij}^{nl} such that $\gamma/\alpha \ll 1$, which corresponds to the points in the (s^*, q^*)-plane close to the dashed curve. In our tests, the condition number of τ_{ij}^{nl} was higher than 20 in about 75% of the domain.

The dynamic mixed model exhibits similar trends in figure 5. The key difference between nonlinear and mixed models is that the latter can predict SGS stresses that are not positive definite, i.e. have a negative eigenvalue. In our test this results in about 4% of points below the dashed line. For constant C_s in (4.3), an increase in C_s leads to an increase in the of fraction of τ_{ij}^{mix} that is not positive definite.

The performance of the DS model is shown in figure 6. It is apparent that not only does the DS model gives a good prediction for q^*, it also captures the correct trend as the filter size increases. This leads us to surmise that models based on the

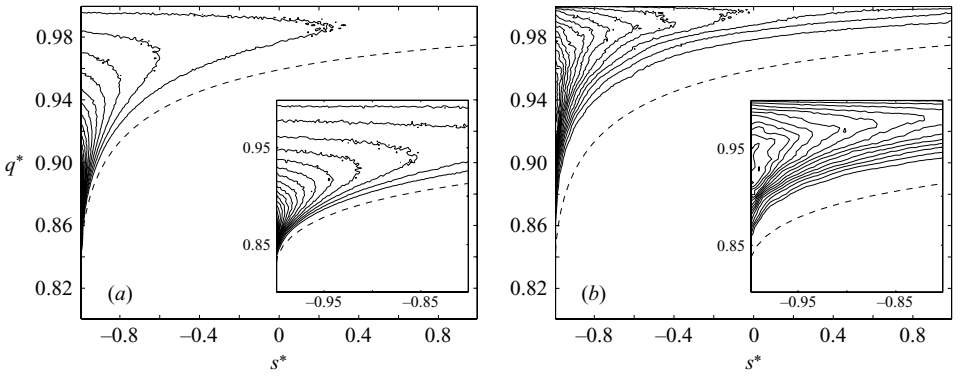

FIGURE 6. Contour plot of $P_{\tau^{ds}}(s^*, q^*)$ for various filter sizes: (*a*) $\Delta = 2\pi/64$, (*b*) $\Delta = 2\pi/16$. The ratio of test and base filter sizes is equal to 2. Fifteen contours are shown, equally spaced from 7.0 to 116.0 in (*a*), and from 3.0 to 59.0 in (*b*).

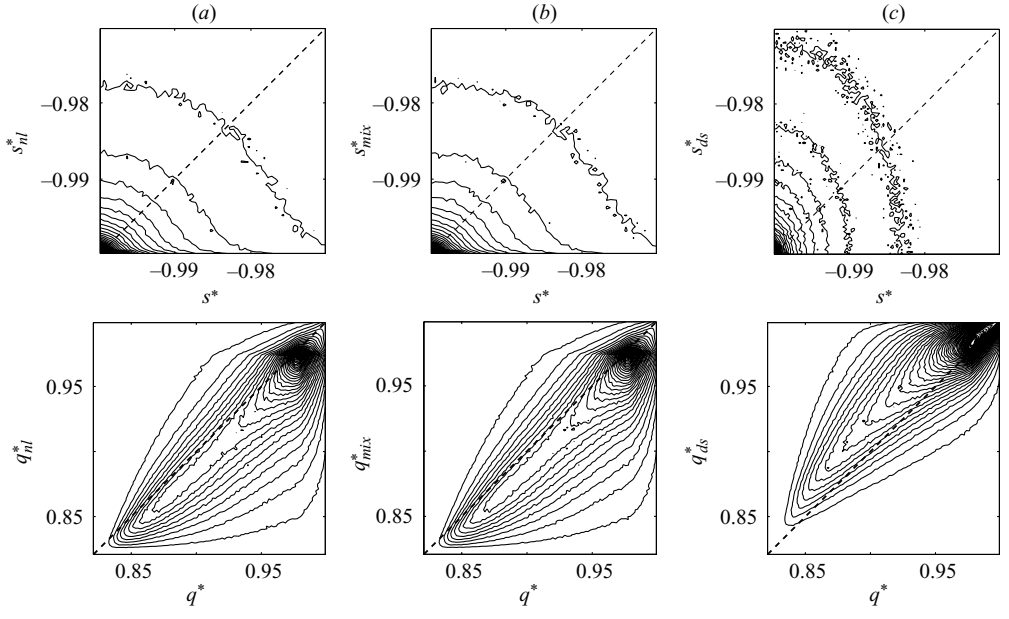

FIGURE 7. Joint PDF of actual and predicted s^* (upper plots) and q^* (lower plots) for (*a*) nonlinear model, (*b*) mixed model, and (*c*) dynamic structure model. Filter size is $\Delta = 2\pi/64$. For the top plots, the difference between adjacent contour values is 100, and the lowest value is 100. For the bottom plots, the difference between adjacent contour values is 10, and the lowest value is 5.

scale-similarity assumption are capable of good prediction of the distribution of the SGS stress configuration for a variety of filter sizes.

It should be noted that the test filter plays an important role in the quality of prediction for the mixed and DS models since their structural terms explicitly depend on the test filter. We have found that for our data the DS model gives the best prediction for $\hat{\Delta}/\Delta \approx 1.3$, but in order not to bias our comparison we set $\hat{\Delta}/\Delta = 2$, as for the mixed model.

So far we have tested the quality of the models' prediction only in terms of distributions. Now we evaluate the prediction of s^* and q^*. This is done in figures 7

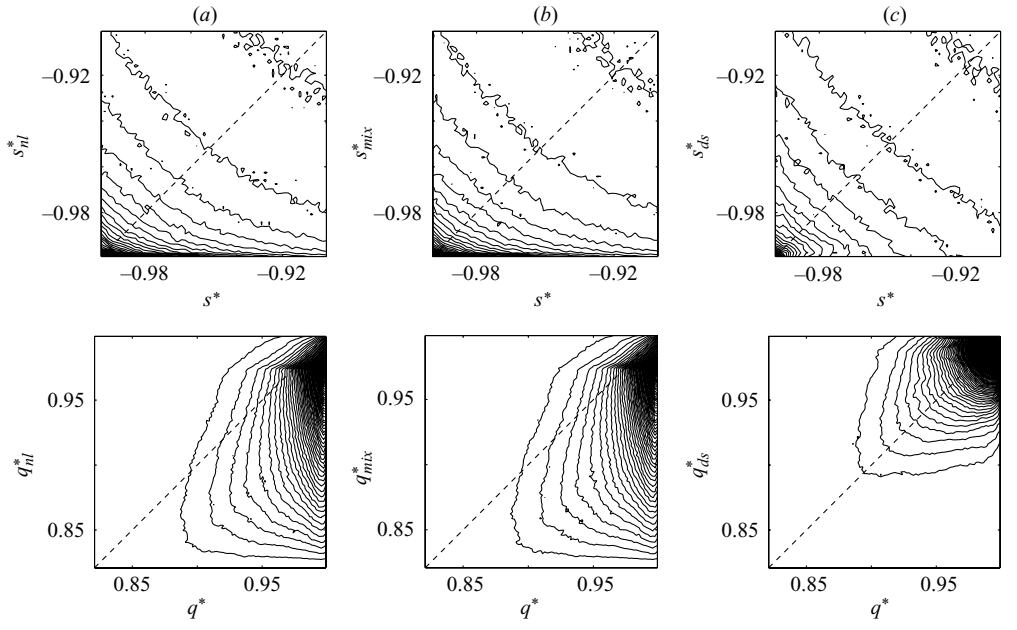

FIGURE 8. As figure 7 but filter size is $\Delta = 2\pi/16$.

and 8 via the joint PDF of the actual and modelled s^* and q^*, for two filter sizes. All joint PDFs for s^* have a sharp peak at $(-1, -1)$, so the neighbourhood of that point is shown.

It is evident from the figures that the Taylor-expansion-based models tend to under-predict s^* and q^* for both filter sizes. While the under-prediction of s^* does not seem to be very significant, the under-prediction of q^* becomes severe for large filter size. A sudden 'step' in the joint PDF of (q^*, q^*_{nl}) and (q^*, q^*_{mix}) at the values of q^*_{nl} and q^*_{mix} of approximately 0.975 is explained by the fact that this is the highest value of q^* on the dashed lines on previous figures, and the PDFs for these models are highly concentrated along the dashed line.

The DS model, on the other hand, tends to over-predict both s^* and q^* for small filter size, but shows symmetric PDFs for both s^* and q^* for larger filter size.

5. Conclusions

We introduce two quantities s^* and q^* that can be used to parameterize the relative distribution of the eigenvalues of any symmetric tensor. The key feature of this parameterization is that both s^* and q^* are uniformly distributed in the space of symmetric matrices and thus the joint PDF of (s^*, q^*) is not biased towards any particular state. Analytical proof and numerical illustration are provided.

Using s^* and q^* we can examine *a priori* the distribution of states of any symmetric tensor. In particular, we consider the SGS stress τ_{ij}, its states and dependence of the state distribution on the filter size. Our tests show that the most probable value of s^* is -1, which corresponds to two repeated smaller eigenvalues, while the distribution of q^* displays a dependence on the filter size Δ. For larger Δ the averaged subgrid scales naturally become more isotropic. When Δ is reduced, values of q^* are highly concentrated close to the boundary which corresponds to singular τ_{ij}. Together with $s^* \approx -1$ this indicates that τ_{ij} has one large and two small eigenvalues, which leads

us to the conclusion that on the smallest scales the most frequent configuration of turbulent flow has one strongly fluctuating and two smooth velocity components.

Using the proposed parameterization we can also evaluate the performance of LES models for τ_{ij}. Four such models are examined: Smagorinsky, nonlinear, mixed and dynamic structure (DS). The models are selected due to their structural differences. A DNS data set of forced, homogeneous, isotropic turbulence is used for *a priori* testing. The tests indicate that the nonlinear and mixed models under-predict both s^* and q^* for various Δ; the predicted τ_{ij} are consistently very close to the singularity curve on the (s^*, q^*)-plane, while the actual τ_{ij} departs from it for larger Δ. This, to our knowledge, is the only reported *a priori* test that the nonlinear model fails. The state prediction of similarity-based models appears to be much closer to actual, especially for larger filter sizes. This leads us to believe that for large Δ, which presumably is of engineering importance, the models that involve the Leonard tensor are capable of better prediction of the structure of τ_{ij} than the models derived by truncation of Taylor series.

The author is grateful to M. Stepanov for stimulating discussions and to D. Livescu for a version of DNS code. This work was funded by the US Department of Energy (W-7405-ENG).

REFERENCES

Ashurst, W. T., Kerstein, A. R., Kerr, R. M. & Gibson, C. H. 1987 Alignment of vortiity and scalar gradient with strain rate in simulated Navier-Stokes turbulence. *Phys. Fluids* **30**, 2343–2353.

Bardina, J., Ferziger, J. H., & Reynolds, W. C. 1980 Improved subgrid scale models for large eddy simulation. *AIAA Paper* 80-1357.

Borue, V. & Orszag, S. 1998 Local energy flux and subgrid-scale statistics in three-dimensional turbulence. *J. Fluid Mech.* **366**, 1–31.

Chumakov, S. & Rutland, C. J. 2005 Dynamic structure subgrid-scale models for large eddy simulation. *Intl J. Numer. Meth. Fluids* **47**, 911–923.

Germano, M., Piomelli, U., Moin, P. & Cabot, W. H. 1991 A dynamic singrid-scale eddy viscosity model. *Phys. Fluids* A **3**, 1760–1765.

Ghosal, S. 1999 Mathematical and physical constraints on Large-Eddy simulation of turbulence. *AIAA J.* **37**, 425–433.

Goutorbe, T., Laurence, D. & Maupu, V. 1994 A priori tests of a subgrid scale stress tensor model including anisotropy and backscatter effects. In *Direct and Large-Eddy Simulation I, Selected Paper from the 1st ERCOFTAC workshop on Direct and Large-Eddy Simulation* (ed. P. R. Voke, L. Kleiser & J. P. Chollet). Kluwer.

Higgins, C. W., Parlange, M. B. & Meneveau, C. 2003 Alignment trends of velocity gradients and subgrid-scale fluxes in the tubulent atmospheric boundary layer. *Boundary Layer Met.* **109**, 58–83.

Kang, H. S., Chester, S. & Meneveau, C. 2003 Decaying turbulence in an active-grid-generated flow and comparisons with large-eddy simulation. *J. Fluid Mech.* **480**, 129–160.

Kang, H. S. & Meneveau, C. 2005 Effect of large-scale coherent structures on subgrid-scale stress and strain-rate eigenvector alignments in turbulent shear flow. *Phys. Fluids* **17**, 055103.

Kerr, R. M. 1985 Higher-order derivative correlations and the alignment of small-scale structures in isotropic numerical turbulence. *J. Fluid Mech.* **153**, 31–58.

Kerr, R. M. 1987 Histogram of helicity and strain in numerical turbulence. *Phys. Rev. Lett.* **59**, 783–786.

Leonard, A. 1974 Energy cascade in large-eddy simulations of turbulent fluid flows. *Adv. Geophys.* **18**, 237–248.

Leonard, A. 1997 Large-eddy simulation of chaotic convection and beyond. *AIAA Paper* 97-204.

Liu, S., Meneveau, C. & Katz, J. 1994 On the properties of similarity subgrid-scale models as deduced from masurements in a turbulent jet. *J. Fluid Mech.* **275**, 83–119.

Livescu, D., Jaberi, F. A. & Madina, C. K. 2000 Passive scalar-wake behind a line source in grid turbulence. *J. Fluid Mech.* **416**, 117–149.

Lumley, J. L. & Newman, G. R. 1977 The return to isotropy of homogeneous turbulence. *J. Fluid Mech.* **82**, 161–178.

Lund, T. S. & Rogers, M. M. 1994 An improved measure of strain state probability in turbulent flows. *Phys. Fluids* **6**, 1838–1847.

Machiels, L. 1997 Predictability of small-scale motion in isotropic turbulence. *Phys. Rev. Lett.* **79**, 3411–3414.

Mehta, M. L. 2004 *Random Matrices*. Elsevier.

Nomura, K. K. & Diamessis, P. J. 2000 The interaction of vorticity and rate-of-strain in homogeneous sheared turbulence. *Phys. Fluids* **12**, 846–864.

Nomura, K. K. & Post, G. K. 1998 The structure and dynamics of vorticity and rate of strain in incompressible homogeneous turbulence. *J. Fluid Mech.* **377**, 65–97.

Pomraning, E. & Rutland, C. J. 2002 Dynamic one-equation nonviscosity large-eddy simulation model. *AIAA J.* **40**, 689–701.

Pope, S. B. 2000 *Turbulent Flows*. Cambridge University Press.

Smagorinsky, J. 1963 General circulation experiments with the primitive equations. I. The basic experiment. *Mon. Weather Rev.* **91**, 99–164.

Tao, B., Katz, J. & Meneveau, C. 2002 Statistical geometry of subgrid-scale stresses determined from holographic particle image velocimetry measurements. *J. Fluid Mech.* **547**, 35–78.